# INTRODUCTION

Monte Carlo transport codes like FLUKA are useful for many purposes, and one of those is the simulation of the effects of radiation traversing the human body. In particular, radiation has been used in cancer therapy for a long time, and recently this has been extended to include heavy ion particle beams. The advent of this particular type of therapy has led to the need for increased capabilities in the transport codes used to simulate the detailed nature of the treatment doses to the various tissues that are encountered. This capability is also of interest to NASA because of the nature of the radiation environment in space.[1] While in space, the crew members' bodies are continually being traversed by virtually all forms of radiation. In assessing the risk that this exposure causes, heavy ions are of primary importance. These arise both from the primary external space radiation itself, as well as fragments that result from interactions during the traversal of that radiation through any intervening material including intervening body tissue itself. Thus the capability to characterize the details of the radiation field accurately within a human body subjected to such external "beams" is of critical importance.

In order to provide this capability by making use of the widest practical application of the known physics, the FLUKA Monte Carlo code has been extended over the last several years to include the ability to simulate heavy-ion interactions more completely.[2] Currently, FLUKA is available with internal event generators that are capable of simulating inelastic nuclear reactions down to an incident lab kinetic energy of ~100 MeV/A.[3] Work is in progress to extend the internal event generator capability all

the way down to the reaction thresholds, as well as to update and improve the existing capabilities on a continuing basis as new data become available.

One common hurdle in the use of all Monte Carlo radiation transport codes is the difficulty of providing the detailed geometry information about the system to be modeled. This is particularly problematic when the object is as complex as the human body. This situation is multiplied in difficulty by the requirement not only for an accurate positional geometric description, but also the absolute need to attach to that positional information the details of the composition and density of the actual material. In cases where the human body is the object of the simulation, the technique of using information from CT-scans has been common, especially where the nature of the incident beam is restricted to electromagnetic radiation and electrons. This is because the primary information from a CT-scan is a measure of the local distribution of electron density in the object scanned. Raw CT-scan files are generally represented as scan layers of fixed thicknesses with data from individual square cells within each sequential layer being given in raster pixel format. The three-dimensional volume element made up of each of these pixels in a given layer is referred to as a "voxel."

In order to be able to accept these raw CT-scan inputs, FLUKA has been modified to allow for the direct embedding of a region composed of these internal voxels within any normal FLUKA geometric description. So for example, one could embed a CT-scan-based voxel human phantom region within a spacecraft that was otherwise described using the normal FLUKA capabilities. Similarly, a CT-scan-based voxel phantom can be embedded in the external laboratory environment geometry description for simulation of accelerator-based exposures.

Unfortunately, by itself, a raw CT-scan is not as useful in providing a basis for the transport geometry when hadronic beams are applied due to the general lack of direct compositional information. This can be remedied if there is some external process whereby the composition can be overlaid. In some cases, like the soft tissue in the human body, the use of a common global generic composition is a very good approximation. However, when dealing with the whole body or large fractions of it this technique produces incorrect results because some organs, particularly bone and the lungs have both notably different compositions and porous structures.

## ASSIGNING COMPOSITION

In order to address these issues, we have explored the development of an algorithm to distinguish bone and lung tissue from the other soft tissues within the body. The additional small problem of the existence of gas pockets, for example in the stomach and bowel, are easily included due to the very dramatic difference in density.

Our intention is to provide a compositional tag for each voxel that is either a generic "soft tissue," that is global for all soft tissue, or one of the special tissue types including hard bone, trabecular bone and porous lung. It should be emphasized that the actual measured densities will be used scaled to the generic composition assigned based on the x-ray cross sections, which are typically proportional to the electron density. For example, the density of each soft tissue voxel can still vary, even though the presumed elemental compositions remains the same.

The challenges for bone and lung tissue are actually of two distinct kinds. First, there is the initial problem of simply distinguishing this tissue from the surrounding soft tissue. This is generally a pattern recognition problem which yields to well-know techniques that take advantage of density variations. Lung tissue is relatively easy to distinguish, but bone is more problematic. The thin "hard bone" shell that surrounds most human bone tissue is filled with an inner trabecular bone that is a combination of hard-bone filaments and a variety of different kinds of marrow. This composite trabecular bone tissue is typically unresolved on many large-scale CT-Scans, and has an average density that can be similar to the surrounding soft tissue. However, the general property that it is internal to the hard-bone shell typically provides a handle on distinguishing it from the external soft-tissue. We have developed several software tools to facilitate the development of these algorithms.

In general the work reported here has been done using two separate sources for CT-scans. The first is a whole-body image of an adult male [2] that has been previously analyzed by hand to assign voxel by voxel the organ membership along with the corresponding material composition. The second image is that of trabecular bone and represents a 1.2 cm cubic volume entirely with the region of trabecular bone with a 40 μm voxel size. In this case, all voxels are identified either as entirely hard-bone or entirely interstitial marrow.[4]

Figure 1 shows the displays employed to develop the appropriate algorithms. Figure 1(a) contains the whole body image where the voxel densities of the slices shown have been displayed as a corresponding linear gray-scale. Figure 1(b) shows the same image processed by a simple density-based algorithm to distinguish the hard bone from

soft tissue. Note that there is a histogram tool towards the top which displays the actual density profile for the vertical cross-hair line and a fit to that profile by the algorithm. The results are displayed for comparison in the image itself. One can see that the hard bone is easily distinguished from the soft tissue in a general sense. The major difficulties are with the boundary voxels and distinguishing the internal trabecular bone from general soft tissue.

The boundary between hard bone and soft tissue can be problematic because the actual physical boundary between the outer hard-bone surface and the surrounding soft tissue generally occurs in the midst of a voxel rather than close to or along a voxel side. The consequence is a density for the voxel that is intermediate between that of the soft tissue and the hard bone. One possibility is to treat this as a special material that is a weighted homogeneous mixture of bone and soft tissue with the weighting being a linear fit based on the intermediate density value itself. This has the seeming benefit of including the effects of the nearby bone or soft tissue, whichever is the minority, in contrast with the our current algorithm which simply uses a mean value as a threshold either to declare the entire voxel as being bone or soft tissue. However, the actual result is to guarantee that almost all tracks traversing the voxel will have to deal with an incorrect mix, as only a small number will actually see the same medium as the average. On the other hand, our algorithm has the benefit that at least some of the tracks will be seeing the correct density. This is the simplest reasonable solution. A more complex solution that may be employed is similar to the one that has been developed to deal with the trabecular bone regions as discussed in the next section.

Figure 1(b) also shows that the lungs are easily distinguished from the surrounding tissue, and even the central region where the major pulmonary arteries and veins enter the lungs, the distinctions are fairly clear. The lung boundaries present the same challenge as does the bone boundary, and are amenable to the same solutions. These simple algorithms are subject to improvement, but given the level of success that has already been achieved by our methods, considerable progress has been made in getting the material properties into the Monte Carlo geometry inputs.

## TRABECULAR BONE POROSITY

The porosity of trabecular bone and the lungs provides its own challenge. In this case, the problem stems from the fact that the details of porosity occur at a scale that is not practical to evaluate in large volume whole-body CT-scans. As such if the voxel is treated as possessing some mean density with a homogeneous composition, then all tracks traversing the voxel with the same pathlength in the voxel will see the identical medium. In reality, the pseudo-random porous nature of the material will actually give rise to a distribution of pathlengths. As we shall show, this distribution can be very directionally dependent in the case of trabecular bone.

Employing the CT-scan image of trabecular bone with 40 μm resolution mentioned in the previous section, several FLUKA runs were performed using rays to determine the actual pathlengths within the hard bone component of the trabecular bone. In FLUKA, rays are imaginary particles that travel in straight lines and can be used to account for the details of the material traversed along their trajectories. This particular

example of trabecular bone possessed about 10% of its voxels as hard-bone with the remainder being treated as vacuum for our purposes here. Hard bone is taken to have a density of 1.920 gm/cm$^2$ and the pathlength distributions are all given in terms of the gm/cm$^2$ of hard bone traversed per cm of total pathlength traversed. The data are limited to rays with a minimum 0.5 cm pathlength in the trabecular bone volume.

Figure 2(a) shows the pathlength distribution for ~100,000 rays which are incident isotropically on the CT-scan volume. It is seen that there are essentially no rays that manage to avoid all hard-bone voxels, and the mean is about 0.1 gm/cm$^2$/cm. Figure 2(b) is an expanded view of the long pathlength tail of the same distribution.

Figure 3(a) shows the result for another 100,000 rays, but for which the direction is strictly vertical, along the axis of the bone. Slightly more than 50% of these rays pass through the full 1.2 cm of trabecular bone without striking any hard bone voxels!.. This implies that strictly along the axis of the bone, the pathlength variation is a very important feature for particle transport. Figure 3(a) shows a similar set of rays, but where the angle with respect to the bone axis is distributed uniformly over a 100 mrad cone. However, note that even this modest angular deviation from the strict longitudinal axis causes a rapid reduction of this anomaly with the result tending towards the isotropic distribution with the virtual disappearance of the zero pathlength rays.

Figure 4 shows the result for a lateral beam (perpendicular to the bone axis) with no angular spread. A comparison with Figure 2(a) shows that the lateral pathlength distribution is comparable to the general isotropic distribution.

Thus, it appears as if a strategy can be deployed wherein the pathlength used is compensated by a normal distribution fit to the isotropic pathlength distribution, with the

provision that for particle directions that are very close to axial along the bone, a second distribution should be used that is a combination of (a) 50% no hard bone, and (b) 50% of twice the standard isotropic pathlength distribution.

To implement this strategy, rather than vary the actual pathlength, the mechanism to be employed within FLUKA will be to provide for a new kind of material that has a variable density. Then when a particle enters such a medium the program will select the density to be used for that particle randomly from a distribution function. This will allow the effect of the porosity of the medium to be properly simulated and the net effect on a traversing beam of charged particles will be to spread out the energy loss effects as well as the other interactions probabilities.

## CONCLUSIONS

FLUKA has the capability to employ a voxel geometry, and that feature can be used to import information directly from raw CT-scan output files. We have developed a simple algorithm to classify tissue into 4 generic categories. These include soft-tissue, hard bone, trabecular bone and porous lung. With that categorization we can assign generic compositions, and actual densities using the measured CT-scan values to scale the density voxel by voxel. Finally, we have explored the structure of trabecular bone in some detail and have determined the pathlength distribution of typical rays in hard bone within that medium. We have highlighted the substantial asymmetry in the distribution as the rays tend to be aligned along the bone's longitudinal axis. It is planned to implement a new type of material within the FLUKA geometry that will allow a variable

density. Such a variable density material will be able to employ a value that is selected from a specified distribution on a track by track basis. A similar approach is anticipated for the treatment of porous lung tissue, but the detailed examination of the pathlength distributions in lung structure is still being explored.

## ACKNOWLEDGMENTS

We would like to acknowledge the use of the so-called "Golem" whole-body CT-scan data set along with the version that resulted from the efforts of Laura De Biaggi in her detailed voxel by voxel assignment of individual organs to that data set. We are also grateful to Professor Gemunu Gunaratne of the University of Houston for providing access to the trabecular bone CT-scan employed as well as for his efforts in producing graphic images of the CT-scan. Finally, we gratefully acknowledge the permission of Professor Michael A.K. Liebschner of the Bioengineering Department of Rice University to use the trabecular bone CT-scan which Professor Gunaratne had obtained from him originally. This work was partially supported by the EC (contract no. FI6R-CT-2003-508842, "RISC-RAD"), NASA (Contracts NAG8-1901 and NAG8-1658) and the Institute for Space Systems Operations at the University of Houston.

## REFERENCES

1. V. Andersen F. Ballarini G. Battistoni, M. Campanella, M. Carboni, F. Cerutti, A. Empl, A. Fassò, A. Ferrari, E. Gadioli, M.V. Garzelli, K. Lee, A. Ottolenghi,

M. Pelliccioni, L.S. Pinsky, J. Ranft, S. Roesler, P.R. Sala and T.L. Wilson, *The FLUKA code for space applications: recent developments.* Adv. Space Res, *in press* (2004).

2. F. Ballarini, M. Biaggi L. De Biaggi, A. Ferrari, A. Ottolenghi, A. Panzarasa, H.G. Paretzke, M. Pelliccioni, P. Sala, D. Scannicchio and M. Zankl, *Role of shielding in modulating the effects of Solar Particle Events: Monte Carlo calculation of physical and "biological" dose in different organs.* Adv. Space Res., in press (2004).

3. Fassò, A. Ferrari, S. Roesler, P.R. Sala, F. Ballarini, A. Ottolenghi, G. Battistoni, F. Cerutti, E. Gadioli, M.V. Garzelli, A. Empl, J. Ranft *The physics models of FLUKA: status and recent developments* CHEP-2003-MOMT005, Jun 2003. 10pp. Talk given at 2003 Conference for Computing in High-Energy and Nuclear Physics (CHEP 03), La Jolla, California, 24-28 Mar 2003. Published in **eConf C0303241:MOMT005,2003** e-Print Archive: **hep-ph/0306267** (2003).

4. Gunaratne, G. and Leibschner, M., *Private Communication* (2004).

FIGURE CAPTIONS

Figure 1. Screen Shots are presented of the software tool developed to assess the performance of the tissue assignment algorithm. Figure 1(a) shows a slice from the "Golem" CT-scan where the raw density values are displayed on a linear brightness scale as pixels. Figure 1(b) shows the result of filtering this image with the simple threshold algorithm. Note the histogram tool that displays the raw data across the slice and the values from the algorithm superimposed. The Z-axis is the vertical body axis and the X-axis is lateral from side to side, with the Y-axis being front to back. Positive Y is in the forward direction from the body's face.

Figure 2. This displays the pathlength distributions in trabecular bone for an isotropic irradiation. All pathlengths included in the plot have a minimum 0.5 cm absolute length, and the results are plotted as $gm/cm^2$ of hard bone per actual cm of pathlength. Figure 2(a) is an enlargement of the long pathlength tail. The distribution fits a normal distribution quite well.

Figure 3. This displays the pathlength distributions similar to those of Figure 1, but for tracks incident along the longitudinal axis of the bone (the Z-axis) in our coordinate system. Figure 2(a), which is a plot for rays strictly parallel to the Z-axis, shows the surprising behavior of possessing a considerable peak at zero pathlength. However, in contrast, Figure 2(b), which has its rays diverging from the Z-axis with this divergence spread uniformly over angle up to 100 mRadians, and the large zero

pathlength peak is entirely missing.

Figure 4. This plot shows the pathlength distribution that results from an exposure to rays that are exactly parallel to one of the axes that is perpendicular (the reference to X-axis here is intended to be a generic axis perpendicular to the longitudinal axis of the bone). Like Figure 3(a), there is no divergence in the beam, but unlike that figure, there is no corresponding zero pathlength peak.

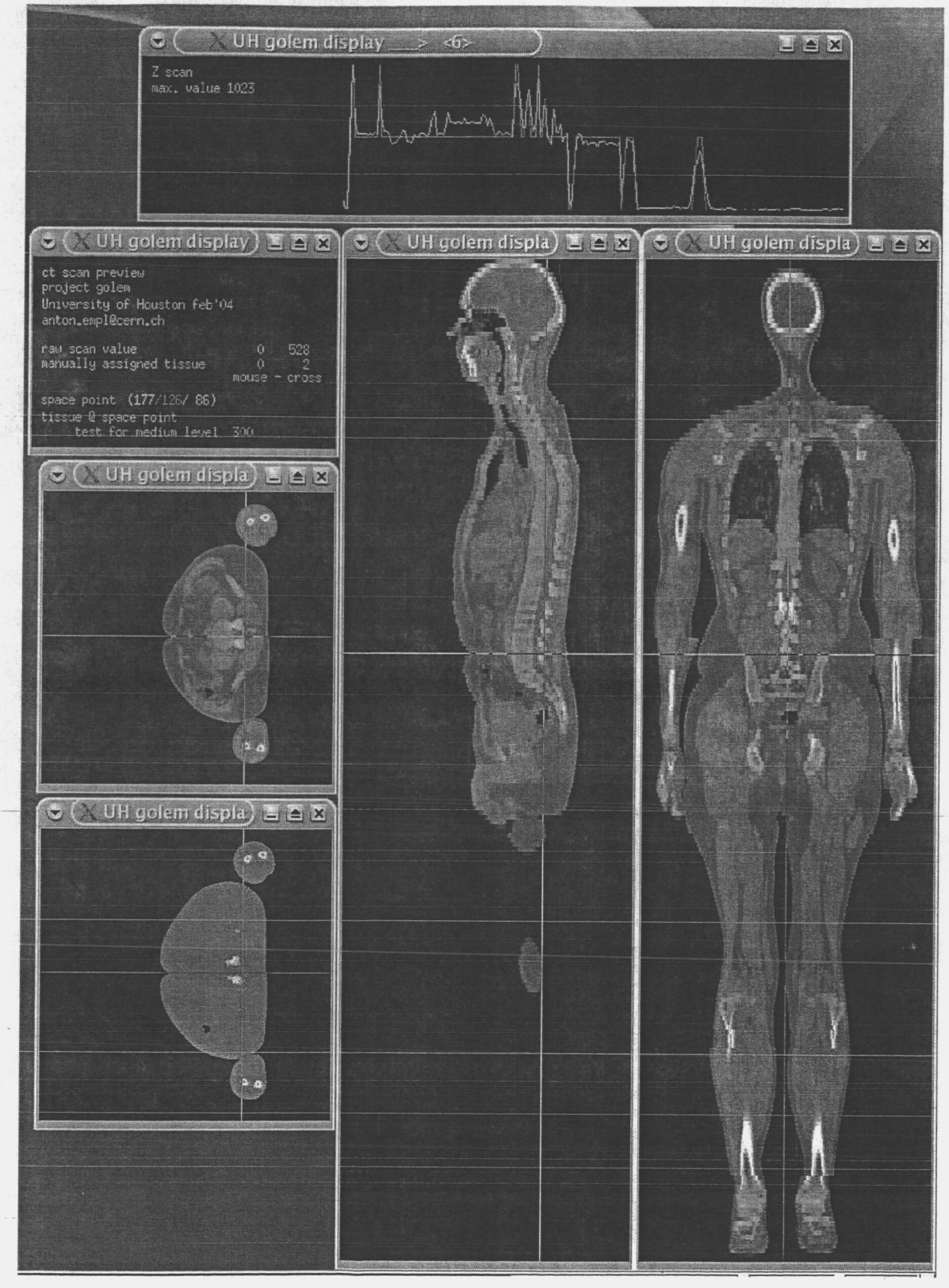
UH golem display ___> <6>
Z scan
max. value 1023
UH golem display
ct scan preview
project golem
University of Houston feb'04
anton.empl@cern.ch
raw scan value 0 528
manually assigned tissue 0 2
mouse - cross
space point (177/126/ 86)
tissue @ space point
test for medium level 300
UH golem displa
UH golem displa
UH golem displa
UH golem displa

Figure 1 (a)

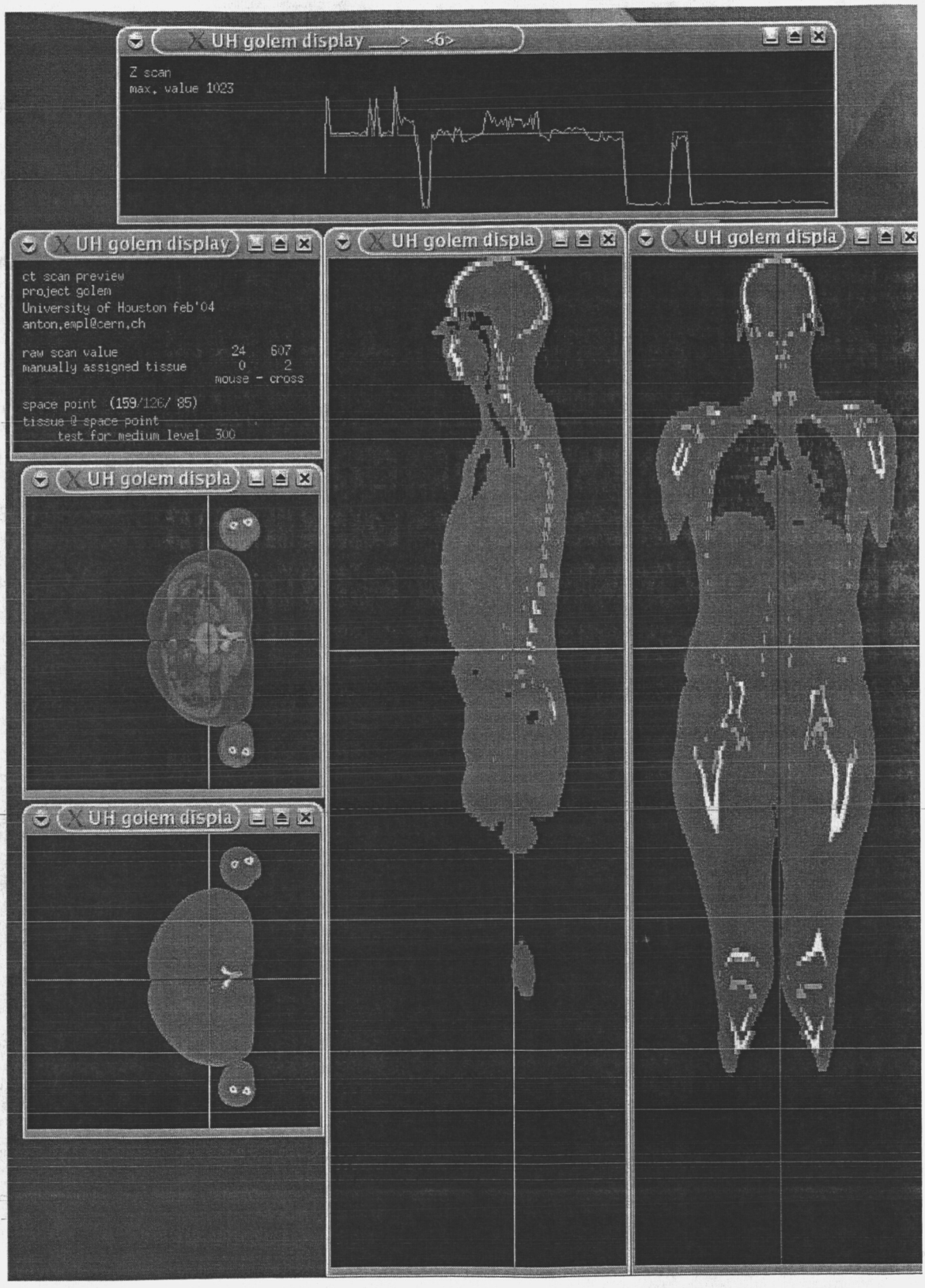
UH golem display ___> <6>
Z scan
max. value 1023
UH golem display
ct scan preview
project golem
University of Houston feb'04
anton,empl@cern,ch
raw scan value 24 607
manually assigned tissue 0 2
mouse - cross
space point (159/126/ 85)
tissue @ space point
test for medium level 300
UH golem displa
UH golem displa
UH golem displa

Figure 1(b)

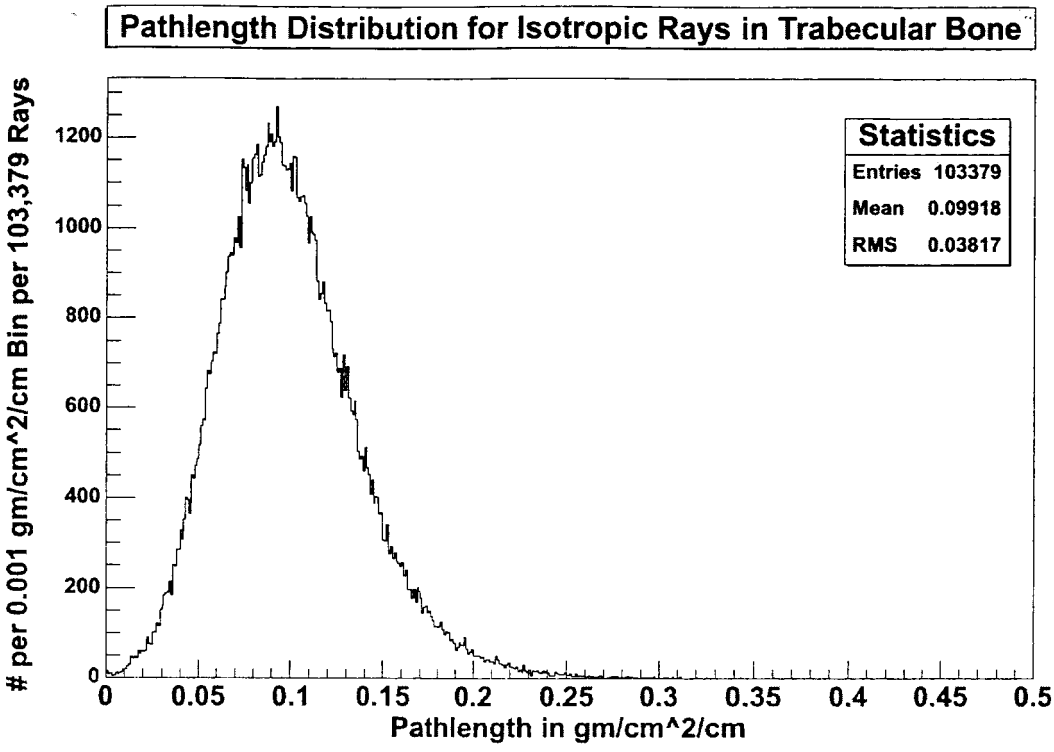


Figure 2(a)

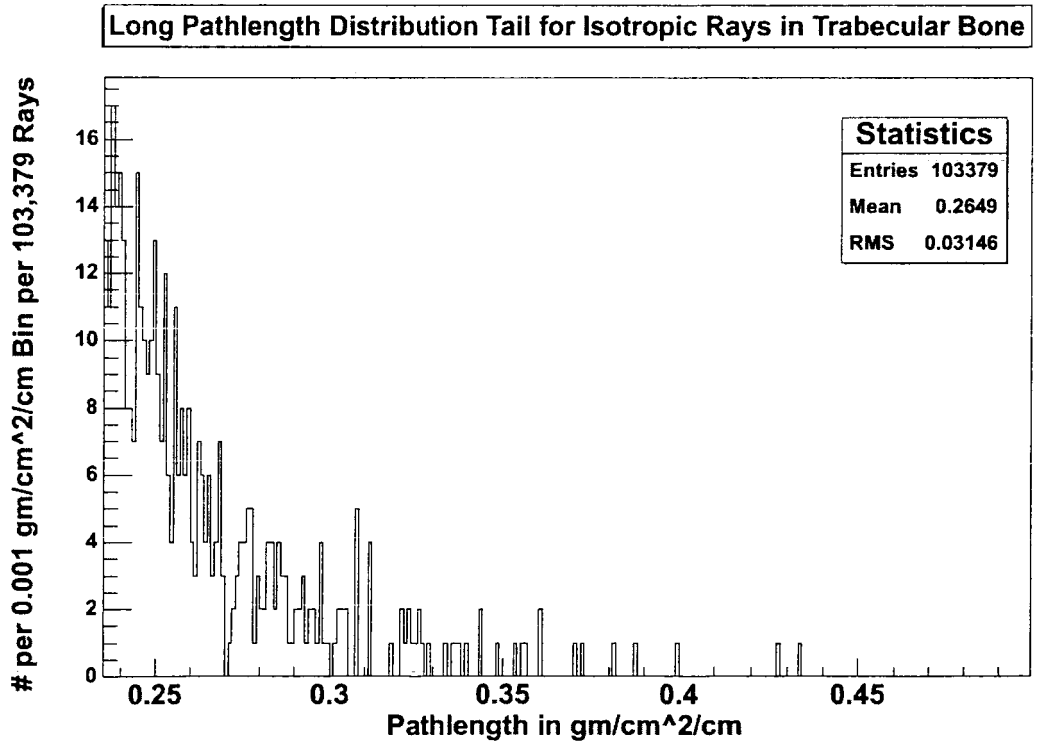


Figure 2(b)

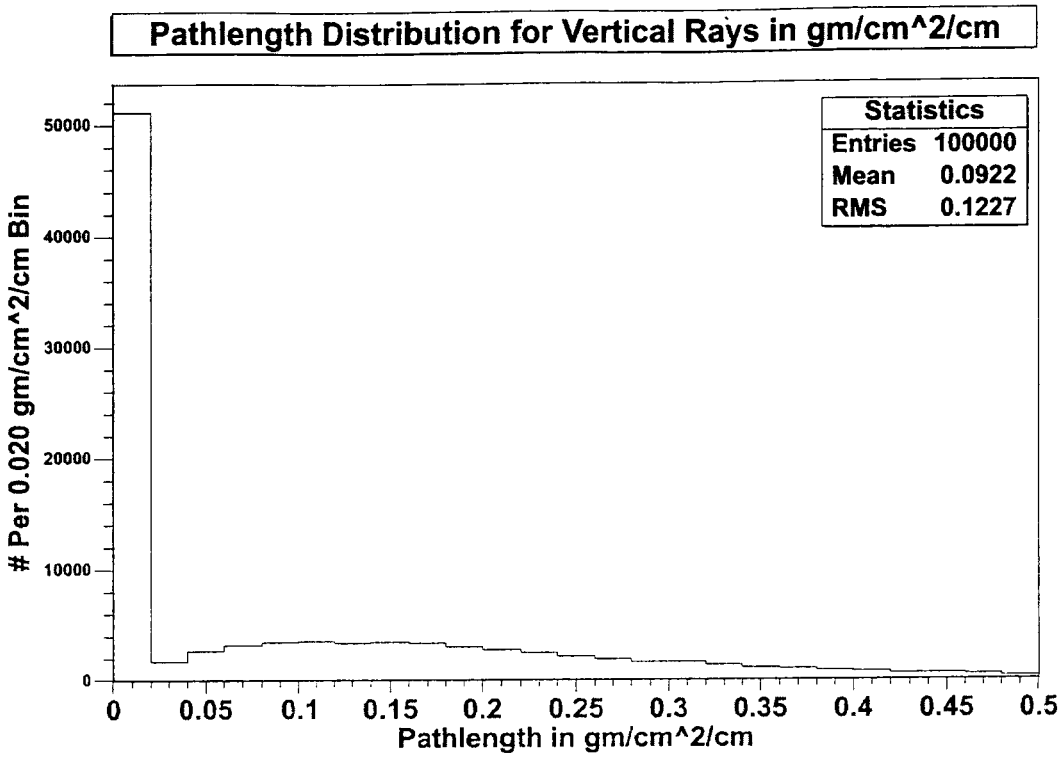


Figure 3(a)

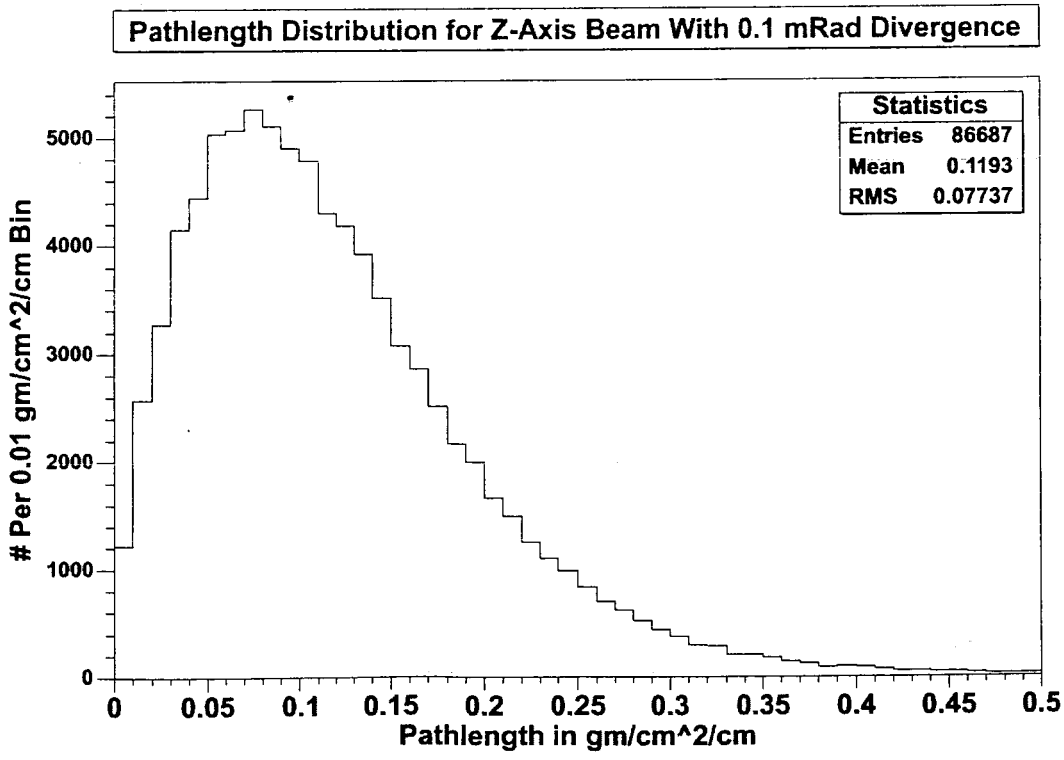


Figure 3(b)

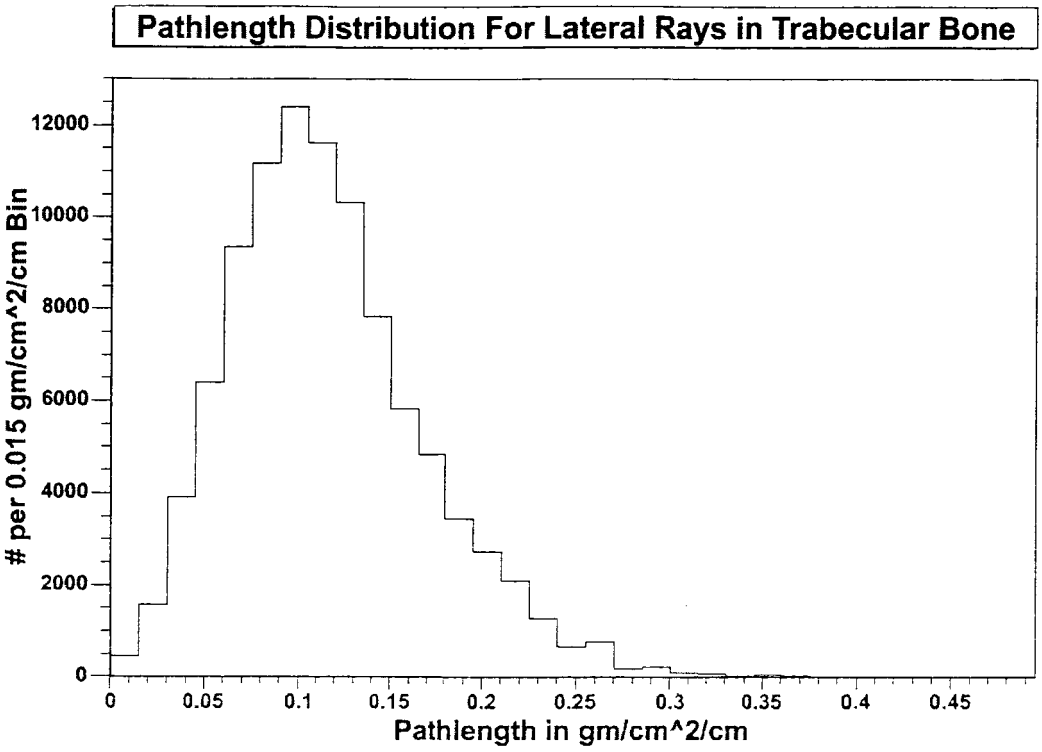
Pathlength Distribution For Lateral Rays in Trabecular Bone
# per 0.015 gm/cm^2/cm Bin
12000
10000
8000
6000
4000
2000
0
0
0.05
0.1
0.15
0.2
0.25
0.3
0.35
0.4
0.45
Pathlength in gm/cm^2/cm

Figure 4

Committees
Topics
Important Dates
Call forPapers
Abstract submission
Abstract reviewing
Preparation of Papers
Tutorials
Proceedings
Sponsors
Conference fees
Registration
Contacts
Accomodation
About Madeira
Home
See the Poster

# ICRS 10 RPS 2004

Madeira, 9-14 May 2004

21st Century Challenges in Radiation Protection and Shielding

Word

## Conference Program

PDF

### Submission of full papers

Please send to icrs-rps@itn.mces.pt one e-mail including:

- The **complete** paper (including figures and tables) in **MS-Word**, or in **.rtf** format
- Each **figure** separately (one file per figure)
- Each **table** separately (one file per table)

**Poster Session Instructions** **Speakers' Instructions**

**Deadline for submission of Papers** ~~30~~ 1st April 2004

- **Contributed papers maximum of 3200 words or 4 printed pages**
- **Invited papers maximum of 4800 words or 6 printed pages**

Joint organization of

Tenth

## International Conference on Radiation Shielding (ICRS-10)

and

Thirteenth Topical Meeting on

## Radiation Protection and Shielding

# (RPS-2004)

## *9-14 May 2004*

## *Funchal, Madeira Island (Portugal)*



maintained by:
Teresa Pires
Juan Manuel Galán

updated 27-04-2004

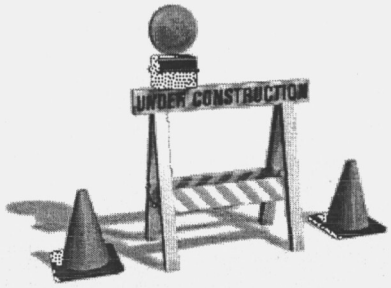


TOP